Integrated reflection and refraction processing of an ultra-shallow seismic survey

Alan Meulenbroek
Velseis Pty Ltd, and School of Earth Sciences, University of Queensland
PO Box 118, Sumner Park
Queensland, Australia 4074
alanm@velseis.com

SUMMARY

Velseis Pty Ltd acquired and processed an ultra-shallow seismic reflection survey designed to image targets with a depth of less than 50m, including the structure of the weathering layer. Several experimental sources were implemented, each with unique frequency and amplitude characteristics.

Reflection processing was not routine since the target of interest was the weathering zone itself. Due to this, a combination of reflection and refraction processing was used in order to develop an integrated image and interpretation of the near-surface.

The results from the different processing techniques, including refraction (reciprocal method and tomography), reflection, and a depth converted stack, provide an internally consistent interpretation of the base of weathering and layering within the weathering.

Key words: Near-surface seismic, refraction, tomography, reflection

INTRODUCTION

Ultra-shallow (<50m) seismic reflection is difficult, mainly due to the interference from other surface related events (refractions, surface waves) and noise (e.g. Steeples, 1998; Steeples and Miller, 1998).

Velseis acquired and processed an ultra-shallow 2D seismic survey on the eastern seaboard of Australia in 2013/2014. The survey consisted of three separate surveys along the same 1km long line. Firstly, a P-wave survey was acquired at 1m group interval into single, 1C geophones. The second and third surveys consist of a converted-wave (PS) survey and a shear–wave (SH) survey, both recorded into 3C geophones.

The data processing approach taken here is somewhat unconventional. Because the aim was not to image a specific target as such, but to develop an image of the overall ultra-shallow structure, several different workflows are combined to develop an integrated interpretation. These include P-wave reflection sections, P-wave refraction analyses (reciprocal method/travel-time tomography), PS-(converted) wave sections, SH-wave sections and MASW (surface-wave dispersion) sections. This paper focuses on the P-wave datasets. The MASW experiment is presented in a companion paper (Strong and Hearn, 2015).

SOURCE TESTING AND ACQUISITION

Several P- and S-wave sources were developed and implemented specifically for this survey. Each source possesses a unique combination of technical and logistical advantages and disadvantages. These sources include:

- Conventional 12lb sledge hammer with baseplate,
- Pile-driver source (Bigfoot),
- Pneumatic vertical piston,
- Pneumatic shear-wave generator,
- Electric jackhammer with tamping bit,
- Mini-SOSIE,
- Microvibe (I-BEAMs).

The first 4 are impulsive sources where shot records are acquired from discrete impacts. In practice, the signal-to-noise ratio is increased by acquiring multiple hits at the same source location and stacking the results.

The simplest of these sources is the sledge hammer. However, repeatability can be compromised with operator fatigue. Health and safety risks are also high with the repeated swinging of a large mass having the potential to cause injury.

The pneumatic sources are highly repeatable. The kinetic energy per shot is easy to quantify based on knowledge of source parameters (e.g. Hearn, et al., 1991). Although the pneumatic P-wave source was technically competitive, other sources were preferred for logistical reasons. The pneumatic shear-wave generator was used for the S-wave survey.

The pile-driver source (Bigfoot) combines the repeatability and relative operator safety of the pneumatic source with the ease of use of the sledge hammer. Made in-house, it consists of a long crow-bar with a metal base-plate welded to one end. A star-picket driver is used to hit the top of the crow-bar repeatedly.

The coded-impact sources include the electric jackhammer and conventional Mini-SOSIE. The jackhammer is conceptually similar to the Mini-SOSIE source. Because it is lighter, there is potential for a broader bandwidth signal, and this was observed on some test records. The need for 240V is a disadvantage however. In the field, this was achieved using a 2KW inverter.

An experimental small-scale controlled-frequency source was also developed for this survey. This source is similar to that detailed in Pugin et al. (2013) in that multiple I-BEAM VT-300 tactile transducers are mounted to a plate. However, rather than mounting the I-BEAMs on top of each other, we mounted four of them on the corners of a steel plate with enough space left to park a vehicle on top to obtain ground coupling. Various frequency sweeps and pseudo-random binary sequences were tested. Again, this prototype source was technically attractive, but other sources were preferred for logistical reasons.

The line was located beside a busy roadway with frequent traffic. To reduce the effect of this traffic noise, a short acquisition time was required. In addition, there was a limited time window allowed to acquire each shot. It was found that Mini-SOSIE had the best combination of frequency content and penetration. However, Bigfoot provided the faster acquisition time, as well as adequate penetration and bandwidth characteristics required for this particular survey.

The line was acquired with 400 channels live, at 1m group interval, shot every two stations (100 fold nominal).

P-WAVE PROCESSING

Unless stated otherwise, results shown below are presented relative to the surface elevation, rather than to a flat datum. In this ultra-shallow environment, projecting to a flat datum is particularly sensitive to the choice of replacement velocity. To avoid the introduction of false structures, no re-datuming has been applied.

Figures 1 and 2 illustrate bandpass-filtered (5-10-180-240Hz) shot records from near the start and end of the line. The near-surface geology is clearly different between these two records. Figure 1 exhibits strong traffic noise on the far offsets. A very shallow, high-velocity layer is visible near the shot-point. At longer offsets, the base of weathering refraction starts to become visible. On Figure 2, the direct arrival, base of weathering refraction and what is interpreted to be a refraction off an intermediate layer can be seen. This image also has relatively little coherent noise present. In general, shallow reflection energy is difficult to see on the raw records.

Prior to any processing, it was very important to reduce both coherent and random noise which sometimes dominated the raw shot records. This was done using FK-filters to attenuate the linear noise, and a TFD filter (Hassanpour, 2008) to attenuate the random noise.
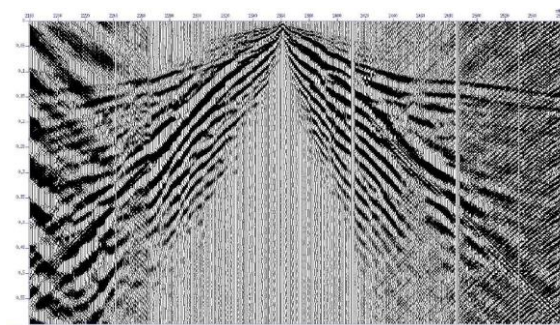

Figure 1. Bigfoot shot record acquired approximately 200m from the start of the line. Maximum offset is 200m and maximum time is 600ms.
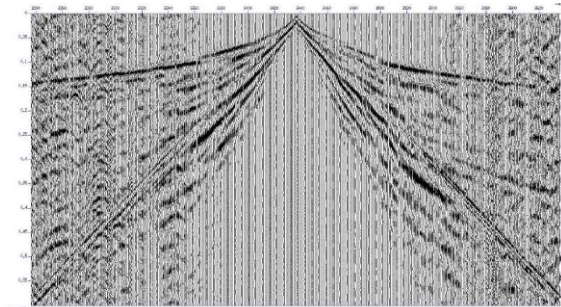

Figure 2. Bigfoot shot record acquired approximately 800m from the start of the line.

Refraction Processing

After noise attenuation, first-breaks were picked and the depths and velocities of each refractor were calculated using the conventional reciprocal method (Hawkins, 1961). Figure 3 shows the depth (from surface) to the top of Layers 2 and 3. The Layer-3 depth was calculated using a constant weathering layer velocity of 500m/s, estimated from near-offset traces.

Velocities of the three layers are shown in Figure 4. The three layers are interpreted to be surface soil (1), intermediate weathered rock (2), unweathered rock (3). Parameters for Layer 2 could not be determined along the whole line due to the absence of reciprocal refraction picks in some areas. This is due in part to the shallow high-velocity layer present at the start of the line. This feature can be seen in the tomographic image (Figure 5) derived by inversion of first arrival times, and on the reflection image discussed below.
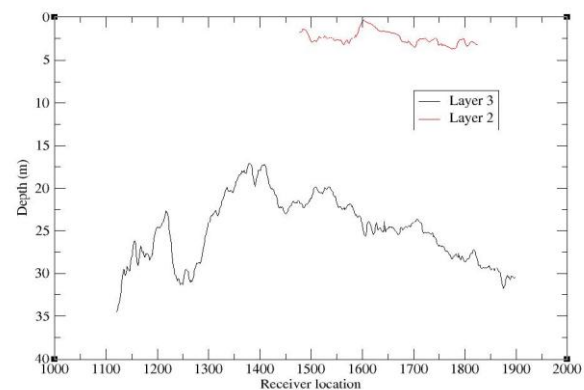

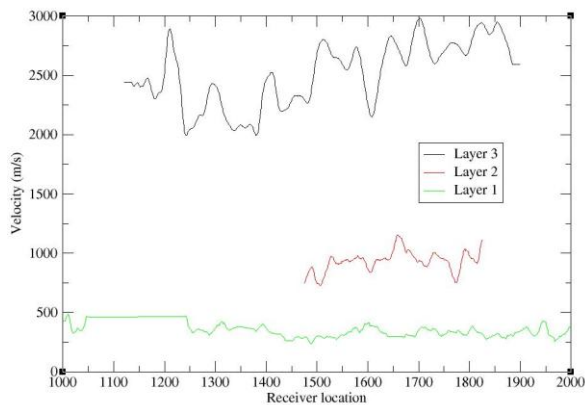**Figure 3. Depth to refractor, derived from reciprocal analysis.**

Figure 4. Refraction layer velocities. V_1 (green) was estimated from near-offset traces, V_2(red) and V_3 (black) from reciprocal analysis.
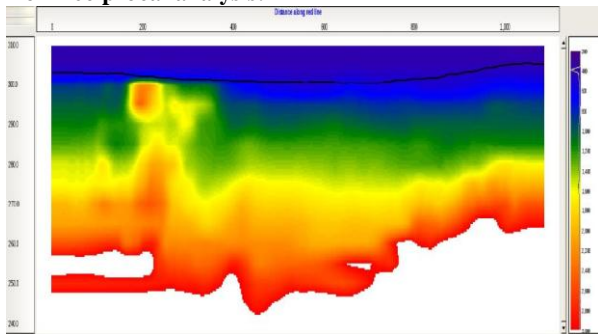

Figure 5. Refraction tomographic solution. Vertical extent=70m. Black curve indicates surface. Maximum velocity (red) = 3000m/s.

Reflection Processing

Processing these data as a conventional reflection survey was not a trivial exercise. It is not simply sufficient to scale down the methods used in deeper prospecting and apply it to the near-surface (Steeples and Miller, 1998). For example, static corrections are not relevant. As noted above, the aim of this survey is to image the structure of the very near surface. Application of weathering static corrections would destroy the desired structure.

Another challenging aspect of processing ultra-shallow data such as this is identifying and separating reflections from refractions (Steeples and Miller, 1998). Figure 6 shows an elastic (no attenuation) synthetic shot record acquired over a model developed from the refraction data. The direct wave, refractions, reflections and ground-roll are all clearly visible, as well as many multiples. Reality is, however, much more complex than models. The S/N in the near-surface can be notoriously low. This coupled with the low dominant frequency of the refracted arrival makes it difficult to exclude refraction energy from the reflection stack.

To clarify this, Figure 7 shows event arrival times for the same model as Figure 6. It is plotted over the same spatial and temporal domains as in Figure 6. The direct wave, PPP refraction and PP reflection are shown as black, red and green curves respectively. The blue curve is the PP reflection corrected using an NMO velocity equal to the surface velocity. As expected, this is flat. The orange curve is the PPP refraction moved-out with the same NMO velocity as the PP

reflection. The timing difference between these two corrected curves does not reach 10ms until approximately 40m offset.

Consider the situation in Figure 7, and assume a refraction with a dominant frequency of 40Hz (T=25ms). An NMO velocity designed to flatten and subsequently stack a reflector will also stack a refraction from the same interface. Although the refraction will stack near the true reflection time, smearing can be expected, due to the low dominant frequency of the refraction. This can be a problem even with severe stretch mutes applied to the data.

In the constant velocity stack of Figure 8, the inclusion of low-frequency refraction energy is obvious (strong event around 100 ms). Steeples and Miller (1998) note that stacking refractions can sometimes lead to a meaningful geological interpretation, even when it is assumed that the event is a reflection. The ray tracing of Figure 7 confirms that the refraction may be at a meaningful time. As seen in Figure 8, however, a major disadvantage is the loss of resolution. One way to significantly exclude refracted energy is to offset limit the data so that the majority of reflections that are recorded are pre-critical reflections, i.e. reflections whose angle of incidence is less than the critical angle. In this region, critically refracted energy is not present and cannot contaminate the stack. This is also desirable from the viewpoint of reflection phase. According to the Zoeppritz equations, at an impedance increase with the incident wave in the upper medium, the phase difference between a reflection from pre-critical and post-critical angles will approach 180 degrees and will tend to destructively interfere. From the refraction data, it was decided that a maximum offset of 30m would eliminate most of the refracted energy. Note that this choice is designed to focus ultra-shallow reflections, but may also discriminate against deeper reflection energy.

Figure 9 shows the improved resolution achieved in the offset-limited stack. For clarity, pre-stack spiking deconvolution was applied to the data. Although in the near-surface almost all of the assumptions of decon are violated. It was more used as an amplitude balancing tool, rather than a multiple removal tool. Post-stack FX-decon was also applied to remove low-velocity effects on the stacked section.

The high-frequency events at approximately 50-60ms at the second half of the line (lower arrow) are reflections from the base of weathering. The lower frequency event at approximately 40ms (upper arrow) is interpreted to be residual refracted energy present from within the 30m offset region. The shape of the reflected energy on the second half of the line compares favourably to the refractor depth profile in Figure 3. Reflection energy from the base of weathering on the first half of the line is very difficult to see due to the low energy transmission through the shallow, high velocity layer. The shallow, high frequency event at approximately 20-30ms corresponds to the shallow, high velocity event in the refraction tomography image of Figure 5.
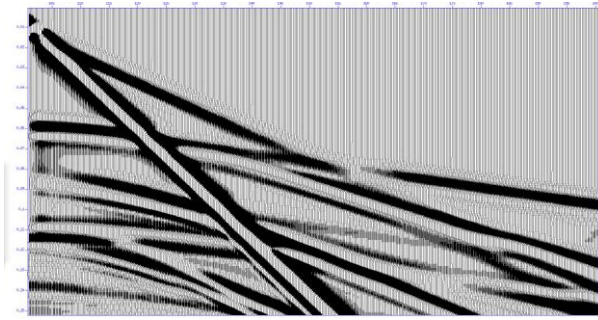
Figure 6. Elastic synthetic shot record showing direct wave, refracted wave, reflection and groundroll.
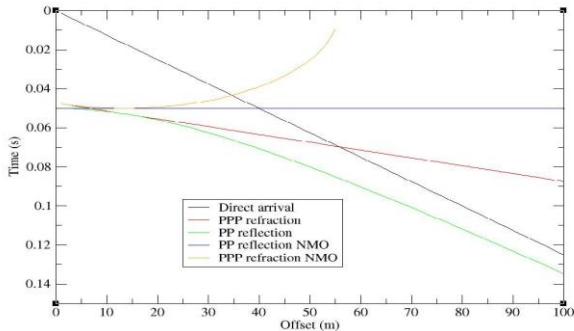

Figure 7. Ray-tracing showing direct arrival (black), refracted arrival (red), reflection (green), NMO corrected reflection (blue) and refraction (yellow); V_{NMO}=800 m/s.
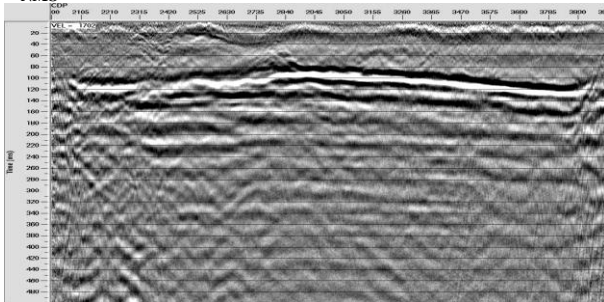

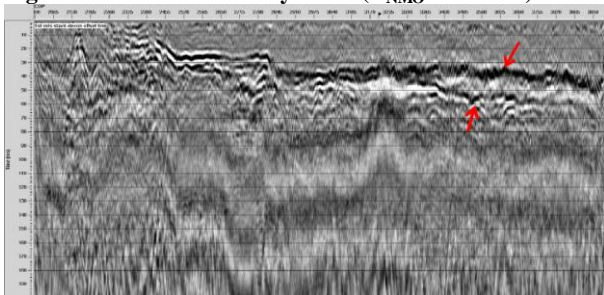**Figure 8. Constant velocity stack (V_{NMO}=1702m/s).**

Figure 9. Offset-limited stack with velocities picked. The top arrow indicates stacked refracted energy. The bottom arrow indicates reflected energy off base of weathering.

Depth Conversion

One objective of this project is to integrate the P-wave data with S-wave information. Comparing events arising from the same interface on different stacks is difficult because of differences between P- and S-wave velocities. One way to overcome this is to create a depth section. This requires a velocity model of the near-surface. In this case, the tomography result (Figure 5) was used as the velocity model.

Figure 10 shows a preliminary depth conversion of Figure 9. The depth of the reflection from the base-of-weathering is very similar to the depth derived from reciprocal analysis (Figure 3). The shallow, high-frequency event has been projected deeper than expected. Rather than the expected depth of 5m (measured from shot records), it projects to approx. 15-20m. This error is caused by the smoothed nature of the tomographic image and higher than expected velocities close to the surface. An improved velocity model is being investigated. Note also that following depth conversion, the apparent reduction in frequency content on some events (e.g. the deeper reflector to the right) is the result of increasing velocities with depth.
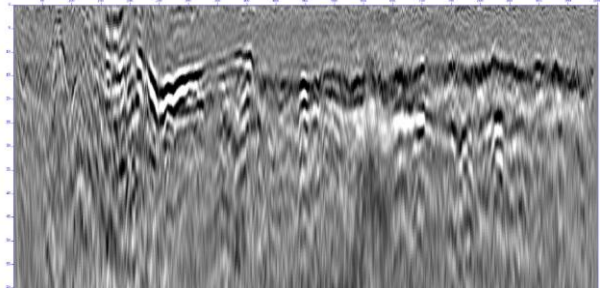

Figure 10. Figure 9 converted to depth. The maximum depth is 60m and the depth increment is 5m.

INTEGRATED INTERPRETATION

A comparison of the offset limited CMP stack, the CMP stack with refractions present, and the depth profile developed from reciprocal analysis and tomography shows that the base of weathering is being imaged by several processes. The concept of allowing refractions to stack is of interest, in that it can provide a relatively simple indicator of approximate near-surface structure. However, such a stack does destroy fine detail. Rejection of refraction energy (e,g, by offset limiting) provides a much higher resolution image of the near surface.

CONCLUSION

Because of logistical constraints, Bigfoot was the preferred source for this survey. In a less noisy situation, Mini-SOSIE would be the preferred source because of its combination of penetration and bandwidth.

Integrated processing of reflection and refraction data is a productive approach for ultra-shallow seismic imaging.

ACKNOWLEDGMENTS

REFERENCES

Hassanpour, H., 2008, A time-frequency approach for noise reduction: Digital Signal Processing, **18**, pp728-738.

Hawkins, L., 1961, The reciprocal method of routine shallow seismic refraction investigations: Geophysics, **26**, pp806-819.

Hearn, S., Kay, M., Dixon, O., 1991, Evaluation of P- and S-wave sources for shallow seismic reflection: Exploration Geophysics, **22**, pp169-174.

Pugin, A., Brewer, K., Cartwright, T., Pullan, S., Didier, P., Crow, H., Hunter, J., 2013, Near surface S-wave seismic reflection profiling - new approaches and insights: First Break, **31**, pp 49-60.

Steeples, D.W., 1998, Shallow seismic reflection section – Introduction: Geophysics, **63**, pp1210-1212.

Steeples, D.W., Miller, R.D., 1998, Avoiding pitfalls in shallow seismic reflection surveys: Geophysics, 63, pp1213-1224.

Strong, S. and Hearn, S. 2015, Can near-surface velocity structure be improved via dispersion analysis of conventional reflection data. ASEG 24th International Conference and Exhibition, Perth.